HAL open science

Experimental and kinetic modeling study of low-temperature oxidation of n-pentane

Bingzhi Liu, Qimei Di, Maxence Lailliau, Nesrine Belhadj, Philippe Dagaut, Zhandong Wang

▶ **To cite this version:**

Bingzhi Liu, Qimei Di, Maxence Lailliau, Nesrine Belhadj, Philippe Dagaut, et al.. Experimental and kinetic modeling study of low-temperature oxidation of n-pentane. Combustion and Flame, 2023, 254, pp.112813. 10.1016/j.combustflame.2023.112813 . hal-04103353

HAL Id: hal-04103353

https://hal.science/hal-04103353v1

Submitted on 23 May 2023

HAL is a multi-disciplinary open access archive for the deposit and dissemination of scientific research documents, whether they are published or not. The documents may come from teaching and research institutions in France or abroad, or from public or private research centers.

L'archive ouverte pluridisciplinaire **HAL**, est destinée au dépôt et à la diffusion de documents scientifiques de niveau recherche, publiés ou non, émanant des établissements d'enseignement et de recherche français ou étrangers, des laboratoires publics ou privés.

Copyright

Experimental and kinetic modeling study of low-temperature oxidation of *n*-pentane

Bingzhi Liu [a,1], Qimei Di [a,1], Maxence Lailliau [b], Nesrine Belhadj [b], Philippe Dagaut [b], Zhandong Wang [a, c*]

[a] *National Synchrotron Radiation Laboratory, University of Science and Technology of China, Hefei, Anhui 230029, PR China*

[b] *Centre National de la Recherche Scientifique (CNRS), INSIS, ICARE, 1C Avenue de la Recherche Scientifique, 45071, Orléans, cedex 2, France*

[c] *State Key Laboratory of Fire Science, University of Science and Technology of China, Hefei, Anhui 230026, PR China*

Abstract: Attractiveness in advanced low-temperature combustion engines drives a constantly updated understanding of low-temperature oxidation chemistry. In this work, the low-temperature oxidation chemistry of *n*-pentane in two jet-stirred reactors at atmospheric pressure and in the temperature range of 500–825 K was investigated using combined analysis methods of synchrotron vacuum ultraviolet photoionization mass spectrometry, gas chromatography, and Fourier transform infrared spectroscopy. Furthermore, the gaseous mixture from JSR was collected in acetonitrile for subsequent product characterization using flow injection analysis, high-pressure and ultra-high-pressure liquid chromatography coupled to a Thermo Scientific™ Orbitrap® Q-Exactive high-resolution mass spectrometry. Numerous intermediate species were identified by these analytical methods, which contributed to unravelling the low-temperature oxidation reaction network of *n*-pentane. A detailed *n*-pentane model was tentatively developed to reduce deviations between experimental measurements and model predictions by updating the rate constants of C_5 keto-hydroperoxide decomposition, C_5 hydroperoxy cyclic ether decomposition, and Korcek reactions of C_5 keto-hydroperoxide, and by introducing pressure-dependent rate constants for the reaction classes of $\dot{Q}OOH + O_2$, $\dot{Q}OOH$ decompositions, concerted $H\dot{O}_2$-elimination of $R\dot{O}_2$, C_5 keto-hydroperoxide decomposition, C_5 hydroperoxy cyclic ether decomposition, and Korcek reactions of C_5 keto-hydroperoxide, and by adding more detailed sub-mechanisms for C_5 cyclic ethers and C_5 keto-

* Corresponding author: E-mail: zhdwang@ustc.edu.cn (Z. Wang)

[1] *Authors contributed equally.*

hydroperoxides. This updated model was validated against a set of available experimental data, including jet-stirred reactor species data and ignition delay times. These exploratory updates of the kinetic model reveal the considerable influence of the rate constants of hydroperoxide decomposition and the pressure-dependent rate constants of key reaction classes on the kinetic model predictions, highlighting the future demands for high-precision quantum chemistry calculations of the pressure-dependent rate constants of the aforementioned reaction classes to reduce mechanism uncertainties and to develop accurate and robust chemical kinetic models.

Keywords: kinetic modelling; pressure dependence; low-temperature oxidation; Korcek reaction; *n*-pentane; keto-hydroperoxides chemistry

1. Introduction

Concerns about the environmental degradation and depletion of energy resources drive the rapid development of advanced internal combustion engines (ICEs). Low-temperature combustion (LTC) is a cleaner and more efficient combustion strategy with promising applications for advanced ICE [1]. The design and evaluation of advanced LTC engines are dependent on accurate chemical kinetic models. Further elucidating the combustion intermediate species of model compounds and clarifying their reaction pathways is crucial to develop accurate reaction mechanisms and to improve model predictions. Experimental data derived from various diagnostic techniques play an essential role in chemical kinetic modelling. The advances in instrumental diagnostic and analytical methods enable the measurement of elusive intermediates, providing insights into the LTC chemistry of model compounds.

n-Pentane is an ideal model fuel for investigating the LTC chemistry of straight-chain alkanes, and its kinetic and thermochemical rules can be applied to larger fuel molecules [2]. Several previous studies have contributed to the pioneering understanding of the oxidation chemistry and kinetic modelling of *n*-pentane, including jet-stirred reactors (JSR) [3], shock tubes (ST) [4, 5], and rapid compression machines (RCM) [6, 7]. Recently, Rodriguez *et al*. [8] investigated the formation chemistry of chain-branching agents during *n*-pentane oxidation in JSRs using three advanced

diagnostic methods, i.e., synchrotron vacuum ultraviolet photoionization mass spectrometry (SVUV-PIMS), laser single-photon-ionization mass spectrometry (SPI-MS), and *cw*-cavity ring-down spectroscopy (*cw*-CRDS). The intermediate evolution of hydrogen peroxide, alkyl hydroperoxides, alkenyl hydroperoxides, keto-hydroperoxides (KHPs), ketene, and diones was followed. Bugler *et al*. [2, 9] carried out ignition time studies of pentane isomers using one RCM and two STs, and developed a detailed kinetic model of pentane isomers by systematically updating the thermochemistry of important species and by evaluating the rate rules of crucial reaction classes. The proposed kinetic model predicts the ignition delay times (IDTs) well over a range of temperatures and equivalence ratio. Subsequently, Bugler *et al*. [10] used gas chromatography (GC) and the *cw*-CRDS method to study species distributions during *n*-pentane oxidation in two JSRs with a temperature range of 500–1100 K, detecting oxygenated species such as C_5 aldehydes, ketones, and diones. The detailed kinetic model was further developed by including several important reaction classes proposed by Pelucchi *et al*. [11] and Ranzi *et al*. [12] and by updating the rate constants of the reaction classes of C_5 hydroperoxyl alkyl radicals to form C_5 cyclic ether. This updated kinetic model mainly improved the prediction of JSRs data, but considerable deviations between experimental measurements and model predictions still remained for some final products and major intermediates, e.g., water (the difference is a factor of ca. 2 at 625 K), 2-pentene (the difference is a factor of >10 at 625 K), propanal (the difference is a factor of ca. 2–3 at 625 K), acetone (the difference is a factor of >10 at 625 K), formic acid (the difference is a factor of >10 at 625 K), acetic acid (the difference is a factor of >10 at 625 K), *etc*. Bourgalais *et al*. [13] recently performed an analysis of intermediates during the low-temperature oxidation of *n*-pentane in a JSR, characterizing a variety of intermediate species using i²PEPICO (double imaging PhotoElectron PhotoIon COincidence). Belhadj *et al*. [14] investigated the species distributions during the low-temperature oxidation of *n*-pentane in a JSR at a pressure of 10 atm. Many oxidation intermediates, such as cyclic ethers, pentanones, diones, alkylhydroperoxides, alkenylhydroperoxides, KHPs, and highly oxygenated molecules (HOMs), were identified using GC, Fourier transform infrared spectroscopy (FTIR), and liquid chromatography coupled to a Thermo Scientific™ Orbitrap®

Q-Exactive high-resolution mass spectrometry (LC-HRMS) analysis. Discrepancies between the experimental results and model predictions for some important intermediates were also observed in the work of Belhadj *et al*. [14], e.g., methanol (the difference is a factor of ca. 2–3 at 640 K), ethanol (the difference is a factor of >10 at 640 K), 1,3-pentadiene (the difference is a factor of >10 at 800 K), formic acid (the difference is a factor of >10 at 640 K), butanal (the difference is a factor of >10 at 640 K), and hydroperoxides (the difference in temperature distributions is ca. 25 – 40K). Therefore, revisiting the low-temperature oxidation chemistry of *n*-pentane is still needed. Indeed, previous studies [2-10, 13, 14] contributed to valuable insights into *n*-pentane oxidation, but further elucidation of the reaction network and understanding of oxidation chemistry to reduce the discrepancies between measurements and model predictions are necessary.

In this work, two JSRs were used to study the low-temperature oxidation of *n*-pentane. Numerous intermediate species were identified by a combined analytical method of SVUV-PIMS, GC, FTIR and LC-HRMS, including $C_5H_{10}O_3$ (KHPs), $C_5H_{10}O$ (cyclic ether), C_5H_{10} (pentene isomers), CH_3CHO (acetaldehyde), C_2H_5CHO (propanal), CH_3COCH_3 (acetone), $C_2H_5COCH_3$ (2-butanone), C_1–C_3 acids, *etc*. These intermediates are crucial for elucidating the oxidation reaction pathways of *n*-pentane and developing an accurate kinetic model. According to experimentally measured intermediates and previously available literature data, a detailed kinetic model of *n*-pentane was tentatively developed by updating the rate constants of hydroperoxide decomposition, by including pressure-dependent rate constants of key reaction classes, and by adding a more detailed sub-mechanism for important intermediate species such as C_5 cyclic ethers and C_5 KHPs.

2. Experimental methods

The low-temperature oxidation of *n*-pentane in JSRs was studied using four analytical methods: SVUV-PIMS, GC, FTIR, and LC-HRMS. The experiments were carried out at the atomic and molecular physics beamline (BL09U) of National Synchrotron Radiation Laboratory (NSRL) and Centre National de la Recherche Scientifique (CNRS). The detailed experimental conditions are summarized in Table 1.

Table 1. The JSR experimental conditions used in this work.

Location	T (K)	*p* (bar)	τ (s)	ϕ	*n*-pentane
NSRL	500–825	1.03	0.75	0.25	0.0075
CNRS	520–760	1.03	0.75	0.25	0.0075

2.1. JSR coupled with SVUV-PIMS

This experiment was carried out at NSRL in Hefei, China, using the JSR-SVUV-PIMS experimental platform to study the low-temperature oxidation chemistry of *n*-pentane. The specific descriptions of the JSR-SVUV-PIMS experimental device can be found in a recent publication [15]; only a brief description is given here.

The *n*-pentane (purity 99.9% from Shanghai Aladdin Bio-Chem Technology Co., Ltd) was vaporized and mixed with Ar (dilution gas) by a controlled evaporation and mixing (CEM) system. The *n*-pentane/Ar mixture is then mixed with O_2 (oxygen) and finally enters into the 78 cm^3 JSR. There are four nozzles with a diameter of 0.3 mm in the JSR sphere, and the gas mixture forms jets through the four nozzles and is evenly mixed. The tapered quartz nozzle is welded to the JSR sphere for SVUV-PIMS sampling. The sampled molecular beam subsequently enters into the SVUV-PIMS to be ionized and analyzed. The mass resolution (m/Δm) of SVUV-PIMS is ca. 4000 at m/z 72 in this experiment. The JSR is heated to the specified temperature by a specially designed tubular heating furnace, and the actual reaction temperature is monitored online by a K-type thermocouple inserted into the outlet of the JSR. The uncertainty of the measured temperature is estimated to be within ± 10 K. The methods of species identification and quantification in SVUV-PIMS analysis can be found in a previous study [16]. The photoionization cross sections (PICSs) used in this work are from an online database [17] and some available literature data [18-23]. Furthermore, the quantification of organic hydroperoxides is essential for understanding low-temperature oxidation chemistry. Battin-leclerc *et al*. [24] improved the quantification of the mole fraction of KHP by considering the contribution of fragmentation, but the lack of available PICS remains an important source of quantitative uncertainty. Recently, Hu *et al*. [22] reported experimentally measured PICS for various hydroperoxides (alkyl

hydroperoxides and 4-hydroperoxy-2-pentanone), enabling quantitative measurements of organic hydroperoxides. In this work, we quantified the mole fractions of C_1, C_2, and C_5 alkyl hydroperoxides, and C_5 KHP during low-temperature oxidation of *n*-pentane using PICSs measured by Hu *et al*. [22]. The uncertainties of the quantified mole fractions are estimated to be within ± 10% for *n*-pentane and O_2, ± 30% for species with known PICSs, and a factor of two for species with estimated PICSs.

2.2. JSR coupled with FTIR/GC/LC-HRMS

This experiment was performed at CNRS in Orléans, France. JSR coupled with FTIR/GC/ LC-HRMS analysis was adopted to study the low-temperature oxidation of *n*-pentane. The details of this experimental platform are described in previous publications [14, 25, 26].

The experiment was carried out in a 35 cm^3 JSR, with N_2 as the diluent gas. The gas mixture in the JSR is sampled by a low-pressure sonic probe, and the sampled mixture is transmitted to the analyzers (FTIR and GCs) via Teflon lines. The FTIR was used to detect and quantify H_2O, CO, CO_2, CH_2O, *etc*. Two GCs were used for detecting and quantifying stable intermediate species. A GC equipped with a DB624 column and flame ionization detector (FID) was used for detecting some oxygenated species, while another GC equipped with a CP-Al_2O_3/KCl column and FID was used for detecting several hydrocarbons. Among them, the GC equipped with a CP-CarboPLOT P7 column and thermal conductivity detector (TCD) was also used to detect O_2 and H_2. In addition, GC/MS was used for species identification according to the NIST Mass Spectrometry database. The uncertainties of the measured reaction temperatures in this experiment were estimated to be within ± 10 K, and the uncertainties of the quantified mole fractions in FTIR/GC analysis were within ± 15%. For carboxylic acids, uncertainties are higher, ca. ± 30%

In order to perform LC-HRMS analyses, the gaseous samples exiting a sampling probe were collected for 75 min in a glass vial containing 25 mL of acetonitrile kept at 273 K. To limit the thermal degradation of dissolved samples, they were stored at 258 K in a freezer for future chemical analyzes. Flow injection analysis (FIA) provided a global compound signal with no chromatographic separation. The FIA, high-pressure and ultra-high-pressure liquid chromatography (HPLC, UHPLC) analyses

were coupled to a Thermo Scientific™ Orbitrap® Q-Exactive HRMS. Atmospheric pressure chemical ionization (APCI) produced ions in positive $(M + H)^+$ and negative $(M – H)^–$ modes (see Table S1 in *Supplementary Materials* for details). MS/MS analyses were performed at 10 eV using higher energy collisional dissociation. This analytical method allowed the detection and separation of specific oxygenated intermediates and products, providing additional qualitative information. In the current work, dozens of oxygenated intermediates from the low-temperature oxidation of *n*-pentane were characterized by this analytical method, and these intermediates are recorded in detail in Table S1 of the *Supplementary Materials*.

3. Kinetic model

The detailed chemical kinetic model NUIGMech1.1 [27] served as the starting point of the *n*-pentane model updates in this work. The *n*-pentane sub-mechanism in NUIGMech1.1 [27] is derived from the previously published *n*-pentane model [2, 9, 10], and it was developed by systematically updating the thermochemistry of important species and rate rules of key reaction classes. Although the *n*-pentane model was validated against various experimental data, some inconsistencies between model predictions and measurements drive further model development, e.g., the reactivity of *n*-pentane overestimated at 550–650 K, the considerable deviations between model predictions and experimental measurements for C_5 KHP, CH_3COCH_3, formic acid, *etc*. Details of the model update in this work are given in the next paragraphs.

The rate constants for the reaction class of $\dot{Q}OOH + O_2$, $\dot{Q}OOH$ decompositions, and concerted $H\dot{O}_2$-eliminations of $R\dot{O}_2$ are critical for the low-temperature oxidation reactivity and autoignition behavior of hydrocarbons, as they directly determine the branching ratios of chain propagation and chain branching pathways. Previous publications [28-32] highlighted the pressure dependence of the rate constants of these reaction classes, but high-pressure limit rate constants were used for these reaction classes in NUIGMech1.1 [27]. In this updated model, the rate constants at 1 atm for the reaction classes of $\dot{Q}OOH + O_2$, $\dot{Q}OOH$ decompositions, and concerted $H\dot{O}_2$-eliminations of $R\dot{O}_2$ are tentatively added, with an estimated factor of ca. 2–3 slower than their high-pressure limits.

KHPs are critical chain branching agents that directly control autoignition chemistry. Although numerous experimental studies of KHPs during the low-temperature oxidation of many hydrocarbons and oxygenated fuels have been reported [23, 33-35], studies on the kinetic parameters of KHPs in the literature are scarce, leading to considerable uncertainty in kinetic models. In the case of *n*-pentane, the rate constants of C_5 KHP decomposition from the Polimi model [12], LLNL model [36], NUIGMech1.1 [27], and the presently updated model are compared as a function of temperature in Fig. 1a. The model-predicted mole fractions of C_5 KHP obtained with NUIGMech1.1 [27] using the rate constants of Fig. 1a are shown in Fig. 1b, with the measured C_5 KHP signal profile scaled to the updated model for facilitating comparison. It can be observed that the faster rate constant of C_5 KHP decomposition corresponds to the earlier formation of C_5 KHP, while the slower rate constant of C_5 KHP decomposition leads to the slower formation of C_5 KHP. Significant deviations in the rate constants and model predictions in Fig. 1 drove the evaluation of the rate constants for C_5 KHP decomposition under experimentally measured constraints.

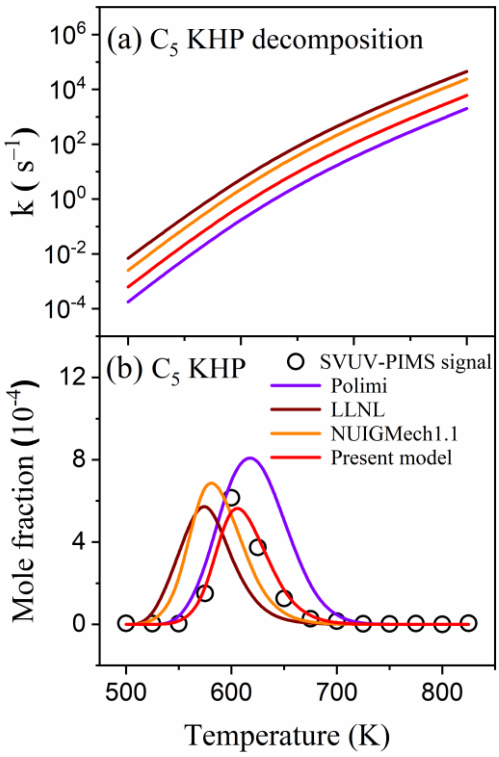

Fig. 1. (a) The rate constants of C_5 KHP decomposition from the Polimi model [12], LLNL model [36], NUIGMech1.1 [27], and the updated model in this work. (b) The model-predicted mole fractions of C_5 KHP derived by NUIGMech1.1 [27] using these rate constants, with the measured C_5 KHP signal

profile scaled to the updated model for facilitating comparison.

A similar approach was recently adopted in the evaluation of the rate constants of C_7 KHP decomposition in the *n*-heptane model [23]. In NUIGMech1.1 [27], the rate constants of the reaction class of C_5 KHP decomposition adopt the O–OH bond scission of heptyl hydroperoxides ($C_7H_{15}O_2H$) experimentally measured by Sahetchian *et al*. [37], but these rate constants are too fast for predicting the C_5 KHP distributions; the prediction is ca. 30 K earlier than the experimental measurements. Moreover, it was noted that several published rate constants of O–OH bond scission of hydroperoxides are a factor of ca. 4 slower than heptyl hydroperoxides measured by Sahetchian *et al*. [37] at 550–750 K, e.g., tert-butyl hydroperoxide [38] and ethyl hydroperoxide [39]. Therefore, the rate constants of the reaction class of C_5 KHP decomposition were decreased by a factor of ca. 4 in the updated model to better predict the measured C_5 KHP distribution at 1 atm. Recently, Goldsmith *et al*. [40] computed temperature- and pressure-dependent rate constants for the decomposition channels of a C_3 KHP using RRKM/ME methods, including the O–OH bond scission and Korcek reactions. The computed results indicated that the rate constants of the O–OH bond scission for KHP at 1 atm are a factor of ca. 2 slower than at 10 atm and for T > 575 K, and the rate constants of the Korcek reactions exhibited considerable pressure dependence. In the updated model, the pressure-dependent rate constants of the O–OH bond scission for C_5 KHP are included, and the rate constant at pressures of 10 atm and higher is estimated to be a factor of ca. 2 faster than that at 1 atm, i.e., the rate constants at 10 atm and higher are a factor of ca. 2 slower than for heptyl hydroperoxides as measured by Sahetchian *et al*. [37]. The pressure-dependent rate constants of the Korcek reactions are updated following the theoretical calculations of Goldsmith *et al*. [40], with a rate constant of 0.17 s^{-1} at 600 K. This is consistent with the calculations (0.16 s^{-1} at 600 K) of Ranzi *et al*. [12]. Recently, Popolan-Vaida *et al*. [41] provided an estimated upper limit of 1.9 s^{-1} at 600 K for the rate constant of Korcek decomposition. Therefore, the rate constant used in the updated model is approximately 10 times smaller than the upper limit estimated by Popolan-Vaida *et al*. [41].

Furthermore, the H-atom abstraction reactions on KHP can form several intermediates, e.g.,

diones, keto cyclic ethers, and olefinic ketones. Xing *et al*. [42] carried out theoretical calculations for the H-atom abstraction reactions of 4-hydroperoxy-2-pentanone in an *n*-pentane oxidation system. Recently, the H-atom abstraction reactions of C_7 KHP and its subsequent reactions were added to the *n*-heptane model by Xie *et al*. [23] based on the calculations of Xing *et al*. [42], to consider the contribution of diones, keto cyclic ethers and olefinic ketones to $C_7H_{12}O$ and $C_7H_{12}O_2$. In this updated model, the H-atom abstraction reactions on C_5 KHPs by $\dot{O}H$, $\ddot{O}$, $\dot{H}$, $H\dot{O}_2$, $CH_3\dot{O}$, $\dot{C}H_3$, $\dot{C}_2H_5$, $\dot{C}_2H_3$, $CH_3\dot{O}_2$ and O_2 were also included according to these previous works [23, 42].

Cyclization reactions of $\dot{Q}OOH$ radicals can lead to cyclic ethers and $\dot{O}H$ radicals. A recent publication [43] reviews the chemical kinetics of cyclic ethers, emphasizing their importance in low-temperature oxidation. Previous studies [44-46] revealed that cyclic ether chemistry enables the potential formation of a variety of intermediate species, such as bicyclic ethers, olefinic cyclic ethers, and diones. In the recent work of Xie *et al*. [23], the predictions of $C_7H_{12}O$ and $C_7H_{12}O_2$ in the temperature range of 625–750 K were significantly improved by adding the detailed C_7 cyclic ether sub-mechanism to the *n*-heptane model. However, the sub-mechanism of C_5 cyclic ethers was not fully detailed in NUIGMech1.1 [27]. 2-Methyltetrahydrofuran and 2,4-dimethyloxetane are the two major cyclic ether intermediates in the low-temperature oxidation of *n*-pentane. In this work, we added the detailed sub-mechanism of these two cyclic ethers to better understand cyclic ether oxidation kinetics. For 2-methyltetrahydrofuran, its sub-mechanism is mainly derived from the published 2-methyltetrahydrofuran model [47], and some reactions and their rate constants were updated in this work according to some available models [23, 47-49]. The 2-methyltetrahydrofuran sub-mechanism mainly includes various pathways of successive additions of radicals to O_2 and subsequent reactions, which leads to olefinic cyclic ethers, bicyclic ethers, cyclic KHPs, *etc*. Especially, Hansen *et al*. [50] recently reported isomer-resolved detection and quantification of cyclic KHPs in the low-temperature oxidation of tetrahydrofuran. For 2,4-dimethyloxetane, its sub-mechanism was added by reference to a previous publication [44] and by analogy with the existing mechanism of tetrahydrofuran and its derivatives [47-49]. The thermochemistry of related species was estimated using the THERM [51].

The 2,4-dimethyloxetane sub-mechanism mainly includes the first and second O_2 addition and subsequent reaction pathways, which leads to olefinic cyclic ethers, bicyclic ethers, diones, cyclic KHPs, *etc*.

$\dot{O}H$ radical addition to acetaldehyde can lead to the formation of formic acid. The rate constant is estimated to be the same as the $\dot{O}H$ radical addition to formaldehyde due to their similar bond dissociation energies. Furthermore, the rate constant of the H-atom abstraction reaction of acetone by the $CH_3COCH_2\dot{O}_2$ radical is estimated to be the same as the H-atom abstraction reaction of acetone by the $CH_3\dot{O}_2$ radical to better predict the formation of acetone.

4. Results and discussion

The detailed pool of species formed during the low-temperature oxidation of *n*-pentane was determined by SVUV-PIMS, GC, and FTIR analysis. It includes hydroperoxides, aldehydes, carboxylic acids, ethers, alkanes, alkenes, and some final products. Furthermore, dozens of specific oxygenated intermediates (see Table S1 in *Supplementary Materials* for details) were characterized by LC-HRMS: C_3–C_5 KHPs, C_5 hydroperoxides, unsaturated C_5 hydroperoxides, 2-butanone, cyclic ethers, diones, HOMs, *etc*. CHEMKIN PRO software [52] was adopted to simulate the experimental results. In low-temperature oxidation, successive O_2 additions of radicals and intramolecular H-atom migration reactions drive the oxidation process. Especially, the exploration of the third O_2 addition reactions contributes to the insights of more complex oxygenated intermediates [53-55]. A previous study [56] demonstrated that the third O_2 addition reaction pathway can accelerate the autoignition of *n*-hexane, but the effect on *n*-pentane is negligible. Therefore, the third O_2 addition reaction pathways were not considered in this work, although the products of the third O_2 addition reactions (e.g., keto-dihydroperoxides) were characterized by LC-HRMS analysis. Scheme 1 describes the reaction pathways of the low-temperature oxidation of *n*-pentane at 600 K, and the dominant reaction pathways, key intermediates and model updates are highlighted. In the following sections, these important reaction classes and the sub-mechanisms of key intermediates are revisited.

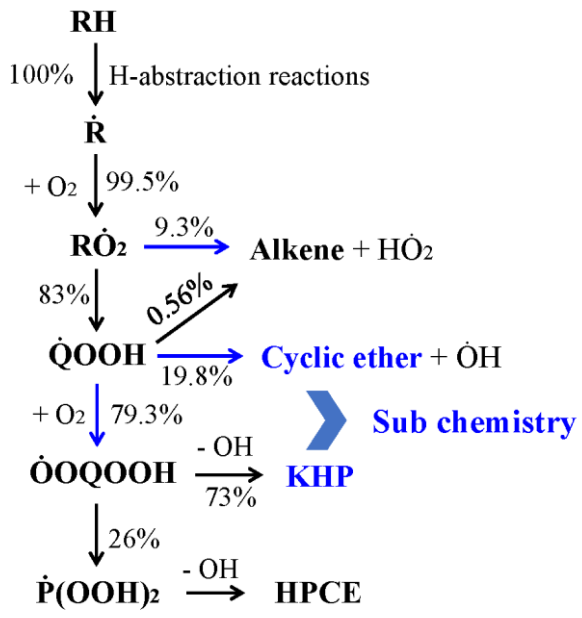

Scheme 1 Reaction pathway analysis during the low-temperature oxidation of *n*-pentane at 600 K. The numbers represent the percentages of the corresponding reaction fluxes. Only the dominant reaction pathways are shown, with the model update highlighted.

4.1 The first and second additions to O_2

As shown in Scheme 1, *n*-pentane forms *n*-pentyl radicals (Ṙ) initially through H-atom abstraction reactions by O_2 and subsequently by radical pools (e.g., ȮH radicals). Ṙ radical addition to O_2 leads to *n*-pentyl peroxy radicals (RȮ$_2$), i.e., the first addition to O_2. RȮ$_2$ radicals dominantly form hydroperoxy pentyl radicals (Q̇ OOH) via intramolecular H-atom migration reactions, accompanied by a competing channel for the formation of the C_5 alkene via HȮ$_2$-elimination reactions. Subsequently, the O_2 addition to Q̇OOH radicals lead to ȮOQOOH radicals, i.e., the second addition to O_2. The ȮH-elimination reactions of ȮOQOOH radicals are responsible for the key intermediate KHP.

Figure 2 shows the measured and model-predicted mole fraction profiles of *n*-pentane, O_2, H_2O, CO, CO_2, 1-pentene (C_5H_{10}-1), 2-pentene (C_5H_{10}-2), and 2-methyltetrahydrofuran ($C_5H_{10}O$1-4) during the low-temperature oxidation of *n*-pentane. Under the present experimental conditions, *n*-pentane showed significant oxidation, with a ~ 50% conversion at 650 K. NUIGMech1.1 [27] overestimates the *n*-pentane reactivity at 550–650 K, which can also be observed in the predictions of some

intermediates shown in Figs. 1-3, Fig. 5, and Fig. S1. The rate constants of the reaction class of $\dot{Q}OOH + O_2$ directly determine O_2 consumption and control the carbon flux to the chain branching pathways; subsequently, the KHP chemistry dominantly drives chain branching chemistry. As shown in Fig. S2, the reaction classes of $\dot{Q}OOH + O_2$ and KHP decomposition have large sensitivity values for the *n*-pentane oxidation reactivity in the temperature range of 550–650 K. The model predictions are improved by updating the rate constants of these reaction classes, i.e., the predictions of *n*-pentane, O_2, CO, H_2O, and other intermediates mole fractions.

The concerted $H\dot{O}_2$-elimination reactions of $R\dot{O}_2$ radicals are the dominant source of pentene isomers, and they have the potential to inhibit ignition by forming relatively unreactive $H\dot{O}_2$ radicals and impact negative temperature coefficient (NTC) chemistry. Two pentene isomers (1-pentene and 2-pentene) were detected and quantified by both SVUV-PIMS and GC; the SVUV-PIMS and GC data are in good agreement. Both models can predict their mole fraction distributions well. The experimental measurements of SVUV-PIMS and GC for 2-pentene in Fig. 2 are the sum of the two isomers (*cis*-2-pentene and *trans*-2-pentene). Neither NUIGMech1.1 nor the updated model in this work distinguishes them. Additionally, the cyclization reactions of $\dot{Q}OOH$ radicals are mainly responsible for the formation of the C_5 cyclic ethers, with $\dot{O}H$ radicals as a byproduct. This reaction is competitive with the second O_2 addition reaction. As shown in Fig. 2h, one dominant C_5 cyclic ether (2-methyltetrahydrofuran) was well separated and quantified by the GC method, and it was also characterized by the LC-HRMS analytical method. Both models can well capture its mole fraction profile.

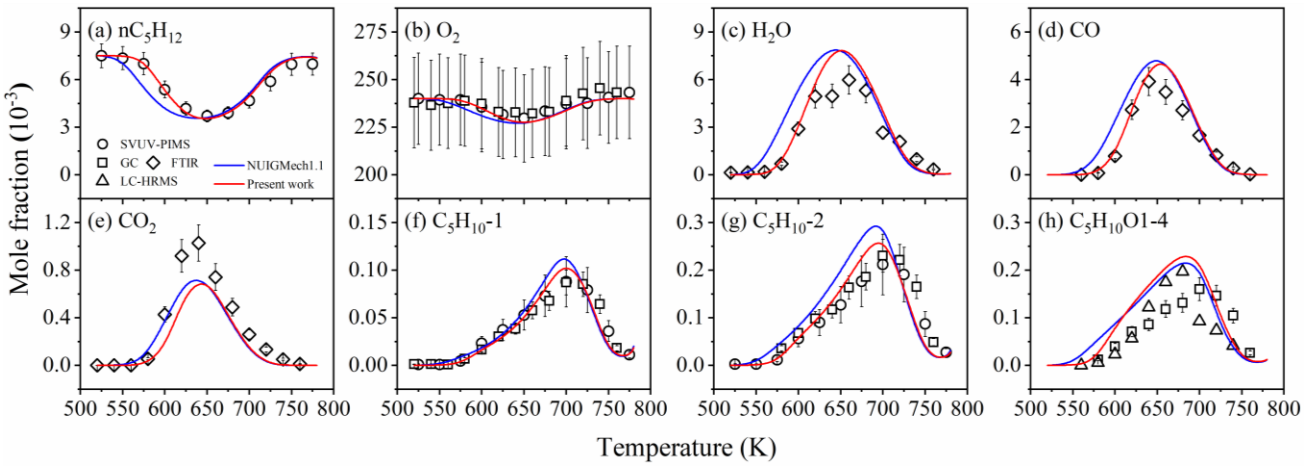

Fig. 2. Experimentally measured (symbols) and model-predicted (lines) mole fraction profiles of *n*-pentane (nC_5H_{12}), oxygen (O_2), water (H_2O), carbon monoxide (CO), carbon dioxide (CO_2), 1-pentene (C_5H_{10}-1), 2-pentene (C_5H_{10}-2), and 2-methyltetrahydrofuran ($C_5H_{10}O1$-4) during the low-temperature oxidation of *n*-pentane. The error bars of SVUV-PIMS, GC, and FTIR data are given. The LC-HRMS measurement were only qualitative; signal profiles were scaled to GC data for comparison.

Furthermore, pentyl hydroperoxide (C_5 ROOH) and C_5 KHP are derived from the subsequent reactions of the first and second additions to O_2, respectively. The reactions between $R\dot{O}_2$ radicals and $H\dot{O}_2$ radicals are responsible for ROOH formation. The subsequent reactions of $\dot{Q}OOH + O_2$ mainly contribute to the production of C_5 KHP (ca. 73% at 600 K), while ~26% yields hydroperoxy cyclic ethers (HPCE), as shown in Scheme 1. In the SVUV-PIMS analysis, the signal of *m/z* 104.084 can be attributed to C_5 ROOH, while the signal of *m/z* 118.063 can be attributed to the combined contribution of C_5 KHP and C_5 HPCE. These highly reactive intermediates are difficult to detect by the GC method, but they can be detected and quantified by SVUV-PIMS method. Since 2-pentyl hydroperoxide and 4-hydroperoxy-2-pentanone are the significant contributors to C_5 ROOH and C_5 KHP during low-temperature oxidation of *n*-pentane, respectively, the mole fractions of total C_5 ROOH and total C_5 KHP/HPCE are estimated here using their PICSs. Figure 3 shows the model-predicted mole fraction distributions of C_5 ROOH, C_5 KHP and C_5 HPCE, and the experimental measured mole fraction distributions of C_5 ROOH and C_5 KHP/HPCE by SVUV-PIMS. Moreover, C_5 ROOH and C_5 KHP were also analyzed by the LC-HRMS method. Since C_5 ROOH and C_5 KHP/HPCE could not be quantified by LC-HRMS analysis, the normalized signal profiles from LC-HRMS were also provided for comparison.

Compared to NUIGMech1.1 [27], the updated model slightly improves the predictions of C_5 ROOH. However, the predictions of C_5 KHP/HPCE from these two models show significant divergences. The prediction of C_5 KHP/HPCE from NUIGMech1.1 [27] is ca. 30 K earlier than the experimentally measured profile. The current model significantly improves the prediction of C_5 KHP/HPCE by updating the rate constants of C_5 KHP/HPCE decomposition and including the pressure-dependent rate constants of $\dot{Q}OOH + O_2$ and C_5 KHP/HPCE decomposition, but still overestimates the mole fraction of C_5 KHP/HPCE by a factor of ca. 3. Because the contribution of HPCE to the formation of $C_5H_{10}O_3$ is not significant from the reaction pathway analysis (Scheme 1), a more detailed HPCE sub-mechanism is ignored in the present model development.

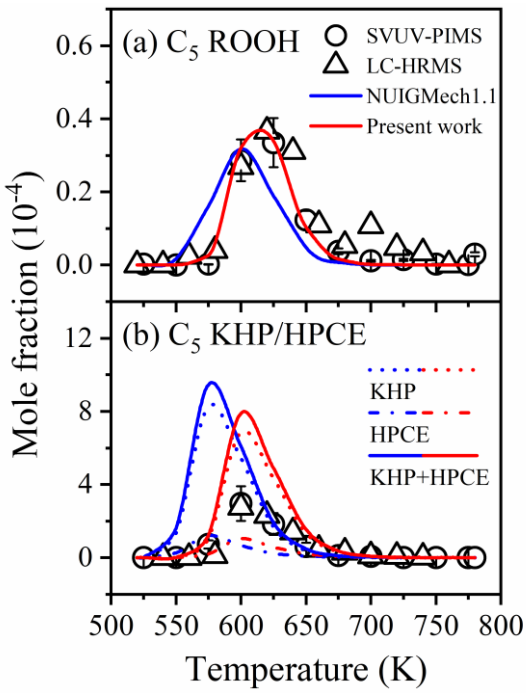

Fig. 3. Model-predicted mole fraction distributions of C_5 ROOH, C_5 KHP, and C_5 HPCE, and the experimental measured mole fraction distributions of C_5 ROOH and C_5 KHP/HPCE by SVUV-PIMS during low-temperature oxidation of *n*-pentane. Since C_5 ROOH and C_5 KHP/HPCE could not be quantified by LC-HRMS analysis, the signal profiles of LC-HRMS were scaled to SVUV-PIMS data for comparison.

4.2 C_5 KHP chemistry

KHP chemistry plays a governing role in the autoignition, knocking, and cool flame chemistry of various kinds of fuels. Currently, three reaction classes of KHP chemistry are commonly adopted.

They include the homolytic O−O dissociation reaction of KHP (hereafter named Reaction class 1), the Korcek reaction of γ-KHP (hereafter named Reaction class 2), and the H-atom abstraction reaction of KHP (hereafter named Reaction class 3). The unimolecular O−O dissociation reaction of KHP leads to the formation of a ketoalkoxyl radical and an ȮH radical. This is the dominant consumption channel for KHP. Additionally, the Korcek reaction is considered a competitive pathway for the chain branching step. Jalan *et al*. [57] determined the γ-KHP decomposition reaction pathways that form cyclic peroxide isomers using ab initio calculations in a propane oxidation system. They indicated that γ-KHP can decompose to carbonyl compounds and carboxylic acids via the Korcek decomposition channel. Popolan-Vaida *et al*. [41] recently provided experimental evidence for carbonyl compounds and carboxylic acid formation through Korcek decomposition of γ-KHP in an *n*-butane oxidation system using the SVUV-PIMS method.

For the H-atom abstraction reactions of KHP, Xing *et al*. [42] performed theoretical calculations for C_5 KHP (4-hydroperoxy-2-pentanone) in an *n*-pentane autoxidation system, showing that this reaction class can lead to crucial oxidation intermediates, such as diones, keto cyclic ethers, and olefinic ketones. To further improve the predictions of the chemical kinetic model, it is necessary to revisit KHPs chemistry. In the case of *n*-pentane, the rate of production (ROP) analysis for C_5 KHP consumption is presented in Fig. 4, highlighting the three aforementioned reaction classes. The C_5 KHP consumption occurs mainly at a temperature of 575–725 K, dominantly through unimolecular O−O dissociation. The other two reaction classes are competing channels of Reaction class 1, and their contribution to KHP consumption becomes negligible with increasing temperature. Even so, Reaction classes 1 and 2 contribute ca. 20% C_5 KHP consumption flux at 600 K.

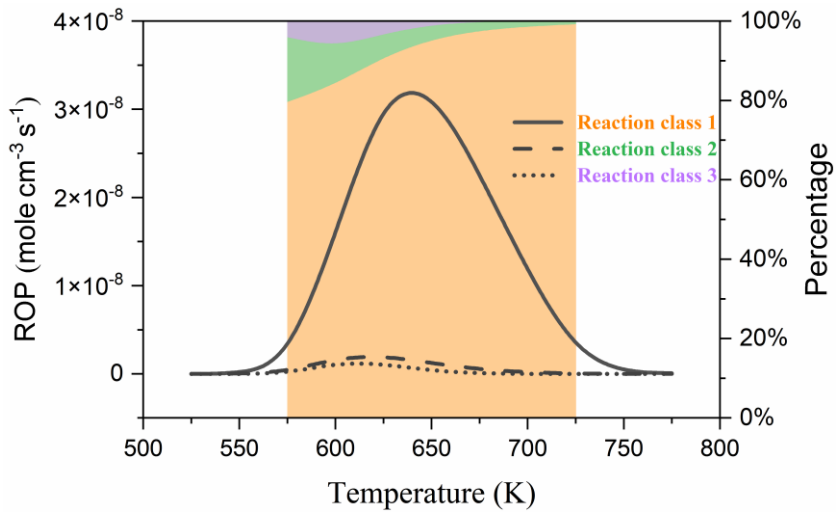

Fig. 4. The ROP analysis for C_5 KHP consumption during low-temperature oxidation of *n*-pentane. The results are based on the simulation of the updated kinetic model in this work. The left coordinate corresponds to the black lines and represents the ROP of these reaction classes. The right coordinate corresponds to the stacked area and represents the percentage contribution of these reaction classes to the C_5 KHP consumption flux. Reaction class 1 represents the homolytic O−O dissociation reaction pathways of C_5 KHP. Reaction class 2 represents the Korcek reaction pathways. Reaction class 3 represents the H-atom abstraction reaction pathways of C_5 KHP.

The *β*-C−C bond scission of the ketoalkoxyl radical derived from the O−O dissociation of KHPs can lead to some small intermediate species. 4-Hydroperoxy-2-pentanone is the dominant C_5 KHP during the low-temperature oxidation of *n*-pentane, and the ketoalkoxyl radical derived from 4-hydroperoxy-2-pentanone is the main source of acetaldehyde and acetone. The *β*-C−C bond scission of this ketoalkoxyl radical directly leads to the formation of acetaldehyde and $CH_3CO\dot{C}H_2$ radicals. The subsequent reaction of the $CH_3CO\dot{C}H_2$ radical forms acetone via a H-atom abstraction reaction. Furthermore, the *β*-C−C bond scission and subsequent reactions of ketoalkoxyl radicals deriving from other C_5 KHPs is one of the formation routes for propanal, 2-butanone, formaldehyde, and methanol. The decomposition reactions of formaldehyde, acetaldehyde, and propanal mainly lead to $H\dot{O}_2$/$\dot{C}H_3$/$\dot{C}_2H_5$ radicals, and the subsequent reactions of these radicals contribute to H_2O_2, CH_3O_2H, and $C_2H_5O_2H$ production. The experimental measurements and model predictions for these intermediate species are presented in Fig. 5. The updated model provides a better prediction of these species but overestimates the mole fraction of $C_2H_5O_2H$ by a factor of ca. 2−3.

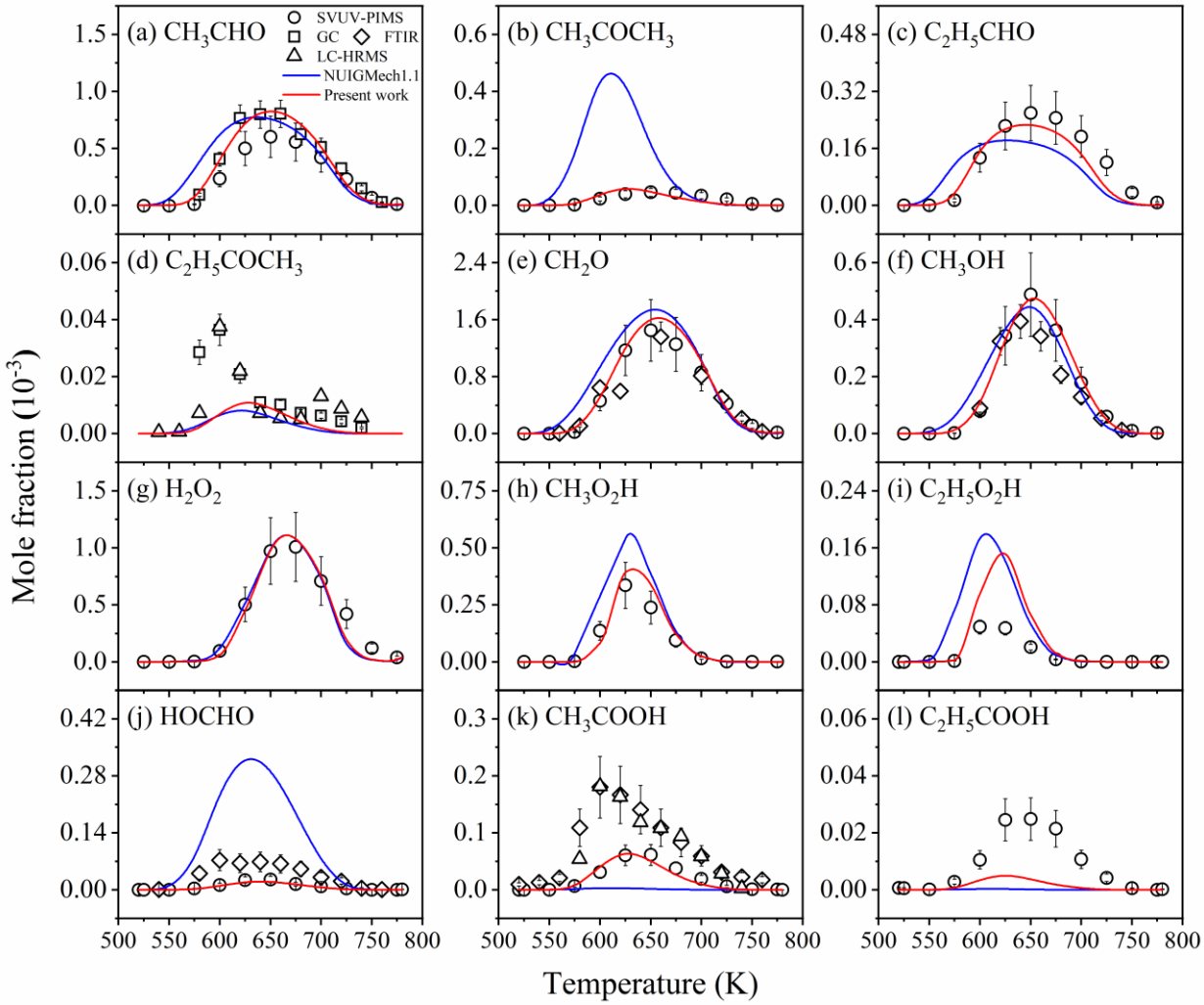

Fig. 5. Experimentally measured (symbols) and model-predicted (lines) mole fraction profiles of acetaldehyde (CH_3CHO), acetone (CH_3COCH_3), propanal (C_2H_5CHO), 2-butanone ($C_2H_5COCH_3$), formaldehyde (CH_2O), methanol (CH_3OH), hydrogen peroxide (H_2O_2), methyl hydroperoxide (CH_3OOH), ethyl hydroperoxide ($C_2H_5O_2H$), formic acid (HOCHO), acetic acid (CH_3COOH), and propionic acid (C_2H_5COOH) during low-temperature oxidation of *n*-pentane. The error bars of SVUV-PIMS, GC, and FTIR data are given. Since LC-HRMS analysis are only qualitative, LC-HRMS signal profiles were scaled to GC or FTIR data for comparison.

Korcek reaction pathways compete with the chain-branching step (Reaction class 1), especially at lower temperatures. The Korcek reactions during *n*-pentane oxidation are presented in Scheme 2, and these reactions can lead to the formation of three carbonyl acids (formic acid, acetic acid, and propionic acid) and four aldehydes/ketones (acetaldehyde, propanal, acetone, and 2-butanone). 4-Hydroperoxy-2-pentanone is the most dominant C_5 γ-KHP, and it leads to the formation of acetic acid and acetone via the Korcek reaction (R3). The measured and model-predicted mole fractions of formic

acid, acetic acid, and propionic acid are presented in Fig. 5. Formic acid and acetic acid were detected and quantified by both FTIR and SVUV-PIMS, but FTIR measurements are a factor of ca. 2 higher than SVUV-PIMS measurements. Additionally, acetic acid was also analyzed by the LC-HRMS method, and the LC-HRMS signal profiles were scaled to FTIR data for comparison.

NUIGMech1.1 [27] overpredicted the mole fractions of formic acid by a factor of ca. 10 and underpredicted the formation of acetic acid and propionic acid. For propionic acid, the presence of the allylhydroperoxide isomer is one of the potential reasons for the inconsistencies between model prediction and experimental measurements. The updated model improved the predictions of formic acid mainly by updating the rate constants of $\dot{O}H$ radical addition to acetaldehyde. Additionally, the rate constant reduction of C_5 KHP decomposition and the rate constant increase of the Korcek reaction lead to more carbon flux to these three carboxylic acids and improve their predictions. As shown in Fig. 6, this branching ratio deviated very large from the calculation of Goldsmith *et al*. [40]. Therefore, a thorough evaluation of the branching ratio of the Korcek reaction, both from experiments and/or theoretical calculations, is believed to help understanding the formation chemistry of carbonyl acids and evaluate the prediction of carboxylic acid.

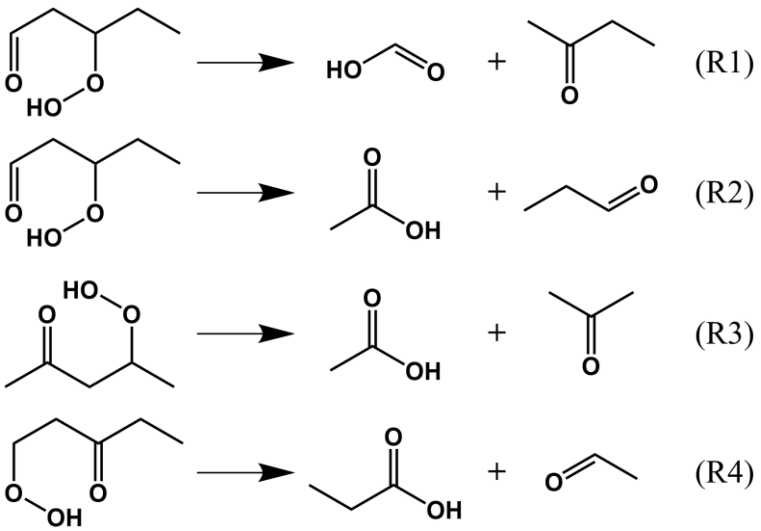

Scheme 2 The Korcek reaction pathways of C_5 γ-KHPs in the *n*-pentane oxidation system.

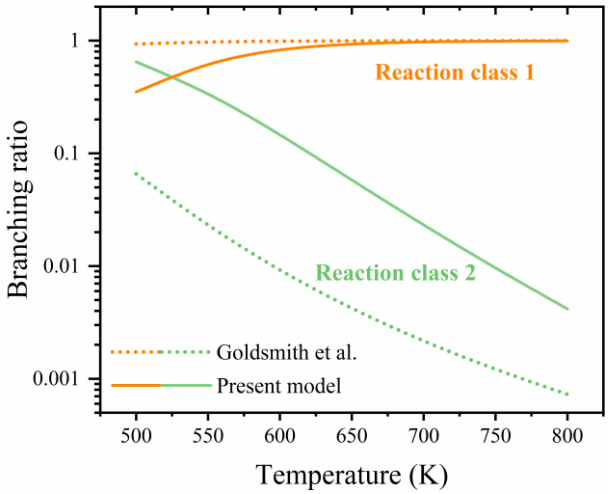

Figure 6. Branching ratio for the rate constants of Reaction class 1 and Reaction class 2 at 1 atm. These rate constants are derived from the calculation of Goldsmith *et al*. [40] and the estimates in this work , respectively. Reaction class 1 represents the homolytic O−O dissociation reaction pathways of C_5 KHP. Reaction class 2 represents the Korcek reaction pathways.

C_5 KHP mainly exists as 4-hydroperoxy-2-pentanone in the *n*-pentane oxidation system, and its H-atom abstraction reactions lead to the production of diones, keto cyclic ethers, and olefinic ketones. As shown in Scheme 3, 4-hydroperoxy-2-pentanone initially forms six radicals at different sites via H-atom abstraction reactions. Subsequently, further $\dot{O}H/H\dot{O}_2$-loss reactions of these radicals lead to the formation of diones, keto cyclic ethers, and olefinic ketones. Different from the diones formed by the *β*-C-C scission of ketoalkoxy radicals, the diones derived from H-atom abstraction reactions of KHP have the same structure as the fuel molecule. The signal profiles of both C_5H_8O and $C_5H_8O_2$ were recorded by SVUV-PIMS, but they contained multiple possible isomers with a wide variety of sources. Since no PICSs are available for these isomers, the total mole fractions of C_5H_8O and $C_5H_8O_2$ are estimated at 11.5 eV using the PICSs of 3-hepten-2-one and 2,3-pentanedione measured by Xie *et al*. [23], respectively. The measured (symbols) and model-predicted (lines) mole fraction profiles of C_5H_8O and $C_5H_8O_2$ are presented in Fig. 7; large deviations between the measurements and simulations were observed if only the H-atom abstraction reaction pathways of C_5 KHP were considered. For the H-atom abstraction reactions of C_5 KHPs, olefinic ketones contribute to the formation of C_5H_8O, while diones and keto cyclic ethers contribute to the formation of $C_5H_8O_2$. The temperature range over which these species are formed is ca. 550−650 K, because they are directly produced from KHP, which is

inconsistent with the SVUV-PIMS measurements of C_5H_8O and $C_5H_8O_2$.

Other reaction pathways can also contribute C_5H_8O and $C_5H_8O_2$, e.g., the oxidation chemistry of C_5 cyclic ethers and pentenes, which will be discussed in the next section. Furthermore, 2,4-pentanedione is separated from the dione isomers and quantified by the GC method, but its mole fraction quantified by GC is higher than the total mole fraction of $C_5H_8O_2$ estimated using SVUV-PIMS data, as shown in Fig. 7b. Interestingly, the mole fraction profile of 2,4-pentanedione is different from the $C_5H_8O_2$ mole fraction profile measured by SVUV-PIMS. Instead, its temperature distribution is the same as that of C_5 KHP (ca. 550−650 K), which indicates that 2,4-pentanedione is mainly derived from C_5 KHP. A similar observation is observed in *n*-heptane low-temperature oxidation, where the authors stated that the diones may come from KHP decomposition in the transfer line from the JSR to the GC analysis [20].

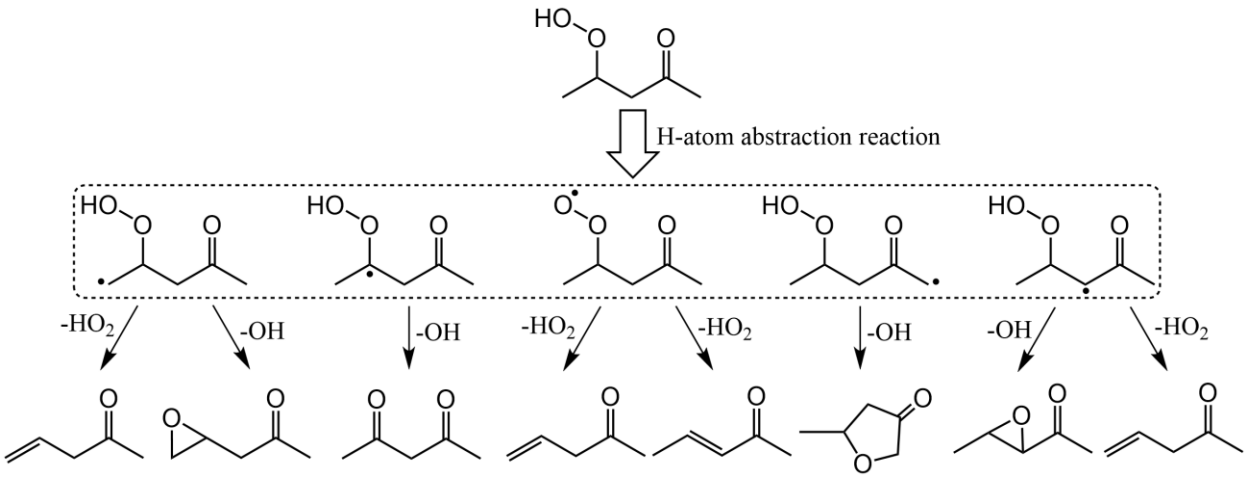

Scheme 3 Reaction pathways of 4-hydroperoxy-2-pentanone leading to diones, keto cyclic ethers, and olefinic ketones via H-atom abstraction reactions.

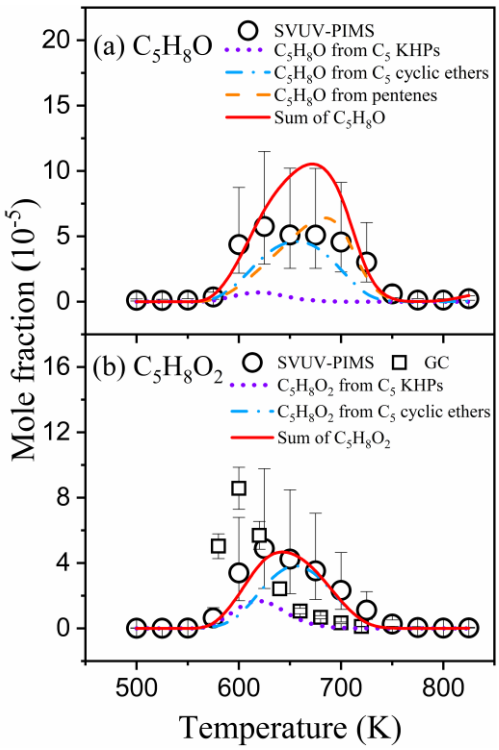

Figure 7. Measured (symbols) and model-predicted (lines) mole fraction profiles of C_5H_8O and $C_5H_8O_2$. Short dot, dash dot and dash lines represent the contributions of the oxidation/decomposition of C_5 KHP, C_5 cyclic ether, and pentene to C_5H_8O and $C_5H_8O_2$, respectively. Solid lines represent their total contributions to C_5H_8O and $C_5H_8O_2$ mole fractions. The error bar for the experimental data is given in the figure.

4.3 The oxidation of pentenes and C_5 cyclic ethers

Alkenes are one of the ubiquitous intermediates in combustion systems, and alkene chemistry can form numerous key oxidation species. ȮH radical addition to the double bond leads to hydroxyalkyl radical formation, which is an important reaction class for alkene chemistry. The O_2 addition reactions of hydroxyalkyl and subsequent β-scission reactions lead to aldehydes production, i.e., the Waddington mechanism. Furthermore, large alkenes (including pentenes) can also undergo successive radical additions to O_2 and intramolecular H-atom migration reactions. In the case of *n*-pentane, 1-pentene and 2-pentene are formed. In NUIGMech1.1 [27], the pentene isomer sub-mechanism has been well established based on the work of Dong *et al*. [58]. The pentene isomers undergo H-atom abstraction, addition to O_2, intramolecular isomerization and subsequent cyclization reactions, leading to the formation of olefinic cyclic ethers, which are the major components of C_5H_8O in Fig. 7a.

The cyclization reaction of the $\dot{Q}OOH$ radical is responsible for the formation of cyclic ethers, and this reaction class has a significant effect on autoignition chemistry. In NUIGMech1.1 [27], the C_5 cyclic ether sub-mechanism has not been well established. 2-Methyltetrahydrofuran is one of the dominant C_5 cyclic ethers in *n*-pentane oxidation. The H-atom abstraction reactions on 2-methyltetrahydrofuran yield five cyclic ether radicals, which could undergo further complex reactions. These dominant reaction pathways for 2-methyltetrahydrofuran to form C_5H_8O and $C_5H_8O_2$ are presented in Scheme 4. Similar to alkane chemistry, O_2 addition to cyclic ether radical forms $ROO\dot{}$ radicals, which lead to the formation of olefinic cyclic ethers via HO_2-concerted elimination reactions or form $\dot{Q}OOH$ radicals via intramolecular H-atom migration reactions. The $\dot{Q}OOH$ radical further reacts via cyclization of the hydroperoxyl group or via ring-opening to form C_5 bicyclic ethers and olefinic esters, *etc*. In the presently updated model, these dominant reaction pathways for O_2 addition to C_5 cyclic ether radicals and the subsequent reactions are included according to recent 2-methyltetrahydrofuran and its derivatives models [47-49]. These reaction pathways mainly contribute to the formation of C_5H_8O and $C_5H_8O_2$ in Fig. 7.

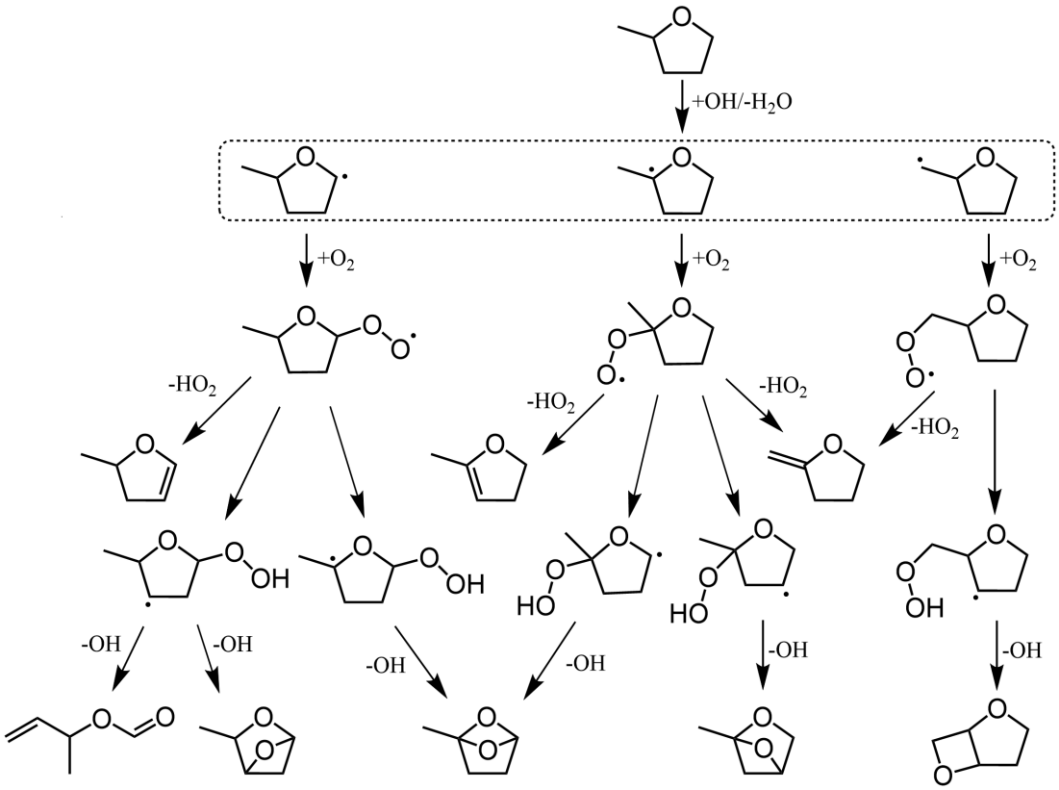

Scheme 4 Reaction pathways of 2-methyltetrahydrofuran to form olefinic cyclic ethers, C_5 bicyclic

ethers, and olefinic esters. Only the dominant reaction pathways leading to C_5H_8O and $C_5H_8O_2$ intermediates are presented.

As shown in Figs. 1 and 2, C_5 cyclic ethers and pentenes are formed at higher temperatures than C_5 KHP during low-temperature oxidation of *n*-pentane. Thus, their oxidation contributes to the formation of C_5H_8O and $C_5H_8O_2$ at higher temperatures. The model satisfactorily captures the mole fraction distributions of C_5H_8O and $C_5H_8O_2$ in Fig. 7 by additionally considering the contribution of the oxidation of C_5 cyclic ethers and pentenes to form C_5H_8O and $C_5H_8O_2$.

Moreover, this updated kinetic model is validated against new measurement data and experimental data available in the literature, including IDTs from both STs and RCMs and JSR speciation data. The model predicts these experimental data well. The detailed model validation is presented in the *Supplementary materials*.

4.4 Hydroperoxides characterized by LC-HRMS

The LC-HRMS analysis characterized numerous elusive oxygenated intermediate species. In this work, in addition to the aforementioned $C_5H_{10}O$1-4, C_5 ROOH, C_5 KHP, $C_2H_5COCH_3$ and CH_3COOH, several hydroperoxides including C_2-C_5 unsaturated ROOHs, C_3-C_4 KHPs and three C_5 HOMs (diketohydroperoxides, unsaturated dihydroperoxides and dihydroperoxides) were also well characterized by the LC-HRMS analytical method. Hydroperoxides are ubiquitous during the atmospheric oxidation of volatile organic compounds and are responsible for the two-stage ignition processes of various fuels. The elucidation of the distribution of hydroperoxide species is helpful for understanding autoignition chemistry.

Figure 8 presents the LC-HRMS signal profiles of these nine hydroperoxide species and the model-predicted mole fraction distributions. Since the LC-HRMS data are only qualitative, the signal profiles of C_2-C_5 unsaturated ROOHs (Figs. 8a-8d) and C_3-C_4 KHPs (Figs. 8e-8f) were scaled to the updated model predictions for comparison, while only the signal profiles of the three C_5 HOMs (Figs. 8g-8i) were given due to the lack of HOM formation pathways in the models. The evolution of these hydroperoxide intermediates indicates that the distributions of C_2-C_4 unsaturated ROOHs and C_3-C_4 KHPs mainly cover the temperature range of ca. 575–650 K. The updated kinetic model satisfactorily

predicts the temperature distributions of C_2-C_4 unsaturated ROOHs and C_3-C_4 KHPs, but prematurely predicts the formation of the C_5 unsaturated ROOH by ca. 100 K. This could be due to the fact we could not differentiate between unsaturated C_5 hydroperoxides and hydroxy-carbonyls. Additionally, the distributions of the three HOM species, i.e., diketohydroperoxides, unsaturated dihydroperoxides and dihydroperoxides, mainly cover a wider temperature range of ca. 575-750 K. Both NUIGMech1.1 [27] and the present model lack formation channels for HOMs and cannot predict their formation. Further development of more detailed kinetic models including the introduction of more complex reaction networks is expected to contribute to the understanding of the formation of these C_5 HOMs.

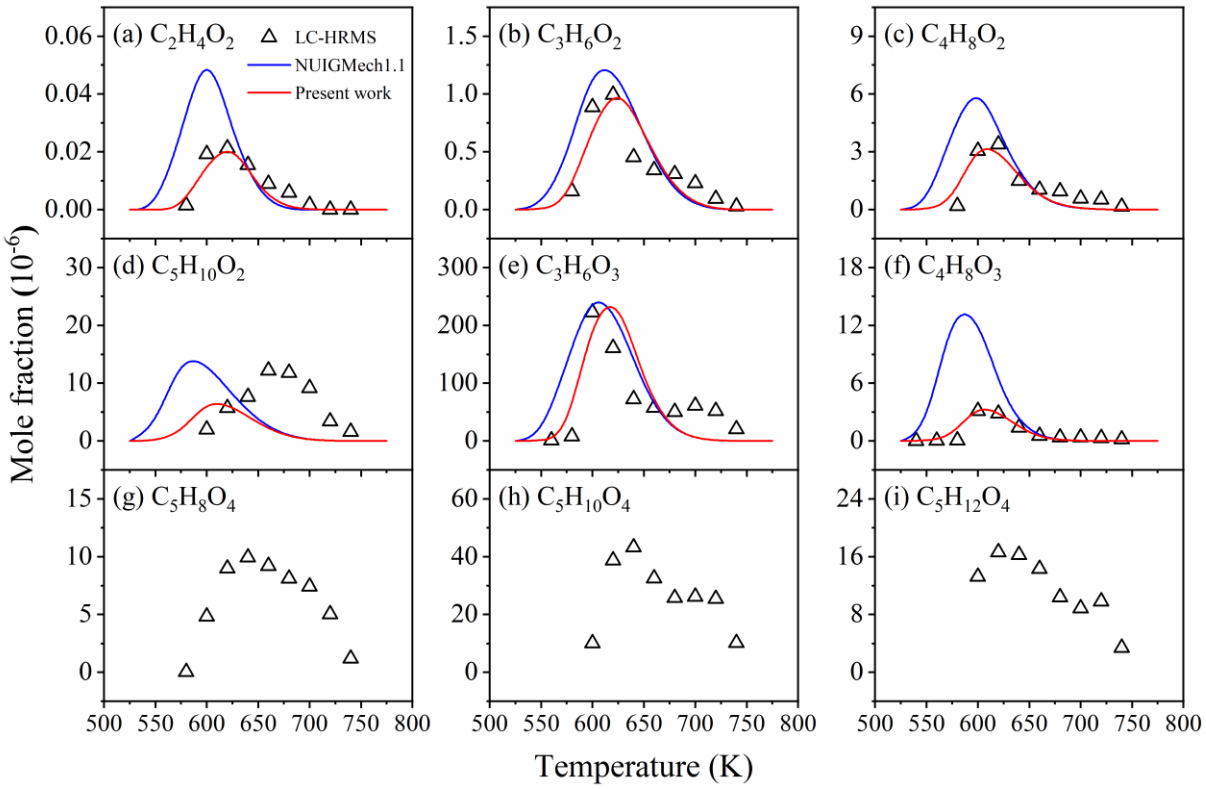

Figure 8. Model-predicted mole fraction distributions and the LC-HRMS signal profiles of C_2-C_5 unsaturated ROOHs, C_3-C_4 KHPs and three C_5 HOMs (diketohydroperoxides, unsaturated dihydroperoxides and dihydroperoxides) during low-temperature oxidation of *n*-pentane. Since LC-HRMS analysis are only qualitative, the signal profiles of C_2-C_5 unsaturated ROOHs and C_3-C_4 KHPs are scaled to the updated model for comparison. The temperature-dependent signal profiles of the three HOMs are also given.

5. Summary and conclusion

The low-temperature oxidation of *n*-pentane in two JSRs at atmospheric pressure and over the

temperature range of 500–825 K was investigated using a combined analytical method of SVUV-PIMS, GC, FTIR and LC-HRMS. Numerous intermediate species were identified, including KHPs, cyclic ethers, H_2O_2, alkyl hydroperoxides, alkenes, aldehydes, ketones, carboxylic acids, *etc*. In particular, LC-HRMS analysis characterized some specific oxygenated intermediates, such as C_3–C_5 KHPs, C_2-C_5 unsaturated ROOHs and several HOMs. These intermediates are used to elucidate the reaction network and update the reaction mechanisms of *n*-pentane oxidation. In the model development, the rate constants of C_5 KHP decomposition, C_5 HPCE decomposition, and Korcek reactions of C_5 KHP are updated. The pressure-dependent rate constants for the reaction classes of $\dot{Q}OOH + O_2$, $\dot{Q}OOH$ decompositions, concerted $H\dot{O}_2$-elimination of $R\dot{O}_2$, C_5 KHP decomposition, C_5 HPCE decomposition, and Korcek reactions of C_5 KHP are tentatively included. Additionally, more detailed sub-mechanisms for C_5 cyclic ethers and C_5 KHP are added. The updated model is validated against measurements in this work and experimental data available from the literature, including JSR species data and IDT data from both RCMs and STs.

These exploratory updates of the *n*-pentane combustion model mainly highlight the governing influence of the rate constants of hydroperoxide decomposition and the influence of the pressure-dependent rate constants of the aforementioned reaction classes on the model predictions. The results in this work indicate that further high-level quantum chemistry calculations for the pressure-dependent kinetics of these reaction classes are necessary to deeply understand the combustion chemistry of hydrocarbon fuels. The introduction of the pressure dependence of important reaction classes and more detailed sub-mechanisms of important combustion intermediates is essential to reduce mechanism uncertainties and to develop accurate chemical kinetic models.

Acknowledgements

This work was supported by National Natural Science Foundation of China (51976208) and the Hefei Science Center, CAS (2020HSC-KPRD001, 2021HSC-UE005). Support from the CAPRYSSES project (ANR-11-LABX-006-01) funded by ANR through the PIA (Programme d'Investissement d'Avenir) is gratefully acknowledged.

References

[1] M. Krishnamoorthi, R. Malayalamurthi, Z.X. He, S. Kandasamy, A review on low temperature combustion engines: Performance, combustion and emission characteristics, Renew. Sust. Energ. Rev. 116 (2019) 109404.
[2] J. Bugler, K.P. Somers, E.J. Silke, H.J. Curran, Revisiting the Kinetics and Thermodynamics of the Low-Temperature Oxidation Pathways of Alkanes: A Case Study of the Three Pentane Isomers, J. Phys. Chem. A 119 (2015) 7510-7527.
[3] C.K. Westbrook, W.J. Pitz, M.M. Thornton, P.C. Malte, A kinetic modeling study of n-pentane oxidation in a well-stirred reactor, Combust. Flame 72 (1988) 45-62.
[4] A. Burcat, K. Scheller, A. Lifshitz, Shock-tube investigation of comparative ignition delay times for C_1-C_5 alkanes, Combust. Flame 16 (1971) 29-33.
[5] V.P. Zhukov, V.A. Sechenov, A.Y. Starikovskii, Self-ignition of a lean mixture of *n*-pentane and air over a wide range of pressures, Combust. Flame 140 (2005) 196-203.
[6] R. Minetti, A. Roubaud, E. Therssen, M. Ribaucour, L.R. Sochet, The chemistry of pre-ignition of n-pentane and 1-pentene, Combust. Flame 118 (1999) 213-220.
[7] R. Minetti, M. Ribaucour, M. Carlier, L.R. Sochet, Autoignition Delays of a Series of Linear and Branched Chain Alkanes in the Intermediate Range of Temperature, Combust. Sci. Technol. 113 (1996) 179-192.
[8] A. Rodriguez, O. Herbinet, Z.D. Wang, F. Qi, C. Fittschen, P.R. Westmoreland, F. Battin-Leclerc, Measuring hydroperoxide chain-branching agents during *n*-pentane low-temperature oxidation, Proc. Combust. Inst. 36 (2017) 333-342.
[9] J. Bugler, B. Marks, O. Mathieu, R. Archuleta, A. Camou, C. Grégoire, K.A. Heufer, E.L. Petersen, H.J. Curran, An ignition delay time and chemical kinetic modeling study of the pentane isomers, Combust. Flame 163 (2016) 138-156.
[10] J. Bugler, A. Rodriguez, O. Herbinet, F. Battin-Leclerc, C. Togbé, G. Dayma, P. Dagaut, H.J. Curran, An experimental and modelling study of n-pentane oxidation in two jet-stirred reactors: The importance of pressure-dependent kinetics and new reaction pathways, Proc. Combust. Inst. 36 (2017) 441-448.
[11] M. Pelucchi, M. Bissoli, C. Cavallotti, A. Cuoci, T. Faravelli, A. Frassoldati, E. Ranzi, A. Stagni, Improved Kinetic Model of the Low-Temperature Oxidation of n-Heptane, Energy Fuels 28 (2014) 7178-7193.
[12] E. Ranzi, C. Cavallotti, A. Cuoci, A. Frassoldati, M. Pelucchi, T. Faravelli, New reaction classes in the kinetic modeling of low temperature oxidation of n-alkanes, Combust. Flame 162 (2015) 1679-1691.
[13] J. Bourgalais, Z. Gouid, O. Herbinet, G.A. Garcia, P. Arnoux, Z. Wang, L.S. Tran, G. Vanhove, M. Hochlaf, L. Nahon, F. Battin-Leclerc, Isomer-sensitive characterization of low temperature oxidation reaction products by coupling a jet-stirred reactor to an electron/ion coincidence spectrometer: case of *n*-pentane, Phys. Chem. Chem. Phys. 22 (2020) 1222-1241.
[14] N. Belhadj, M. Lailliau, R. Benoit, P. Dagaut, Experimental and kinetic modeling study of n-pentane oxidation at 10 atm, Detection of complex low-temperature products by Q-Exactive Orbitrap, Combust. Flame 235 (2022) 111723.
[15] Q. Xu, B. Liu, W. Chen, T. Yu, Z. Zhang, C. Zhang, L. Wei, Z. Wang, Comprehensive study of the low-temperature oxidation chemistry by synchrotron photoionization mass spectrometry and gas chromatography, Combust. Flame 236 (2022) 111797.
[16] O. Herbinet, F. Battin-Leclerc, S. Bax, H. Le Gall, P.A. Glaude, R. Fournet, Z. Zhou, L. Deng, H.

Guo, M. Xie, F. Qi, Detailed product analysis during the low temperature oxidation of n-butane, Phys. Chem. Chem. Phys. 13 (2011) 296-308.
[17] Photonionization cross section database (Version 2.0), National Synchrotron Radiation Laboratory, Hefei, China 2017, http://flame.nsrl.ustc.edu.cn/en/database.htm.
[18] L.G. Dodson, L. Shen, J.D. Savee, N.C. Eddingsaas, O. Welz, C.A. Taatjes, D.L. Osborn, S.P. Sander, M. Okumura, VUV photoionization cross sections of HO_2, H_2O_2, and H_2CO, J. Phys. Chem. A 119 (2015) 1279-1291.
[19] K. Moshammer, A.W. Jasper, D.M. Popolan-Vaida, Z. Wang, V.S. Bhavani Shankar, L. Ruwe, C.A. Taatjes, P. Dagaut, N. Hansen, Quantification of the Keto-Hydroperoxide ($HOOCH_2OCHO$) and Other Elusive Intermediates during Low-Temperature Oxidation of Dimethyl Ether, J. Phys. Chem. A 120 (2016) 7890-7901.
[20] O. Herbinet, B. Husson, Z. Serinyel, M. Cord, V. Warth, R. Fournet, P.-A. Glaude, B. Sirjean, F. Battin-Leclerc, Z. Wang, M. Xie, Z. Cheng, F. Qi, Experimental and modeling investigation of the low-temperature oxidation of *n*-heptane, Combust. Flame 159 (2012) 3455-3471.
[21] B. Dong, Z. Hu, Q. Xu, B. Liu, Q. Zhu, J. Guan, C. Liu, Y. Pan, L. Hu, J. Fang, Z. Wang, Improving quantification of hydrogen peroxide by synchrotron vacuum ultraviolet photoionization mass spectrometry, Combust. Flame 242 (2022) 112214.
[22] Z. Hu, Q. Di, B. Liu, Y. Li, Y. He, Q. Zhu, Q. Xu, P. Dagaut, N. Hansen, S.M. Sarathy, L. Xing, D.G. Truhlar, Z. Wang, Elucidating the photodissociation fingerprint and quantifying the determination of organic hydroperoxides in gas-phase autoxidation, Proc. Natl. Acad. Sci. U. S. A. 120 (2023) e2220131120.
[23] C. Xie, M. Lailliau, G. Issayev, Q. Xu, W.Y. Chen, P. Dagaut, A. Farooq, S.M. Sarathy, L.X. Wei, Z.D. Wang, Revisiting low temperature oxidation chemistry of n-heptane, Combust. Flame 242 (2022) 112177.
[24] F. Battin-Leclerc, J. Bourgalais, Z. Gouid, O. Herbinet, G. Garcia, P. Arnoux, Z.D. Wang, L.S. Tran, G. Vanhove, L. Nahon, M. Hochlaf, Chemistry deriving from OOQOOH radicals in alkane low-temperature oxidation: A first combined theoretical and electron-ion coincidence mass spectrometry study, Proc. Combust. Inst. 38 (2021) 309-319.
[25] C. Togbé, F. Halter, F. Foucher, C. Mounaïm-Rousselle, P. Dagaut, Experimental and detailed kinetic modeling study of 1-pentanol oxidation in a JSR and combustion in a bomb, Proc. Combust. Inst. 33 (2011) 367-374.
[26] P. Dagaut, C. Togbé, Experimental and modeling study of the kinetics of oxidation of ethanol−gasoline surrogate mixtures (E85 surrogate) in a jet-stirred reactor, Energy Fuels 22 (2008) 3499-3505.
[27] A.A. El-Sabor Mohamed, S. Panigrahy, A.B. Sahu, G. Bourque, H.J. Curran, An experimental and kinetic modeling study of the auto-ignition of natural gas blends containing C_1–C_7 alkanes, Proc. Combust. Inst. 38 (2021) 365-373.
[28] X. Yao, W. Pang, T. Li, J. Shentu, Z. Li, Q. Zhu, X. Li, High-Pressure-Limit and Pressure-Dependent Rate Rules for Unimolecular Reactions Related to Hydroperoxy Alkyl Radicals in Normal Alkyl Cyclohexane Combustion. 1. Concerted HO_2 Elimination Reaction Class and β-Scission Reaction Class, J. Phys. Chem. A 125 (2021) 8942-8958.
[29] L. Xing, L. Zhang, F. Zhang, J. Jiang, Theoretical kinetic studies for low temperature oxidation of two typical methylcyclohexyl radicals, Combust. Flame 182 (2017) 216-224.
[30] C.F. Goldsmith, W.H. Green, S.J. Klippenstein, Role of O_2 + QOOH in low-temperature ignition of propane. 1. Temperature and pressure dependent rate coefficients, J. Phys. Chem. A 116 (2012) 3325-3346.

[31] J.R. Duan, J. Ji, L.L. Ye, Y.T. Zhai, L.D. Zhang, A theoretical kinetics study on low-temperature oxidation of n-C_4H_9 radicals, Proc. Combust. Inst. 38 (2021) 681-689.
[32] B. Liu, S. Dong, J. Debleza, W. Chen, Q. Xu, H. Wang, J. Bourgalais, O. Herbinet, H.J. Curran, F. Battin-Leclerc, Z. Wang, Experimental and Updated Kinetic Modeling Study of Neopentane Low Temperature Oxidation, J. Phys. Chem. A 127 (2023) 2113-2122.
[33] F. Battin-Leclerc, A. Rodriguez, B. Husson, O. Herbinet, P.A. Glaude, Z. Wang, Z. Cheng, F. Qi, Products from the oxidation of linear isomers of hexene, J. Phys. Chem. A 118 (2014) 673-683.
[34] J. Bourgalais, O. Herbinet, H.H. Carstensen, J. Debleza, G.A. Garcia, P. Arnoux, L.S. Tran, G. Vanhove, B.Z. Liu, Z.D. Wang, M. Hochlaf, L. Nahon, F. Battin-Leclerc, Jet-Stirred Reactor Study of Low-Temperature Neopentane Oxidation: A Combined Theoretical, Chromatographic, Mass Spectrometric, and PEPICO Analysis, Energy Fuels 35 (2021) 19689-19704.
[35] X.Y. Zhang, Y.Y. Li, C.C. Cao, J.B. Zou, Y. Zhang, W. Li, T.Y. Li, J.Z. Yang, P. Dagaut, New insights into propanal oxidation at low temperatures: An experimental and kinetic modeling study, Proc. Combust. Inst. 37 (2019) 565-573.
[36] S.M. Sarathy, C.K. Westbrook, M. Mehl, W.J. Pitz, C. Togbe, P. Dagaut, H. Wang, M.A. Oehlschlaeger, U. Niemann, K. Seshadri, P.S. Veloo, C. Ji, F.N. Egolfopoulos, T. Lu, Comprehensive chemical kinetic modeling of the oxidation of 2-methylalkanes from C_7 to C_{20}, Combust. Flame 158 (2011) 2338-2357.
[37] K. Sahetchian, A. Heiss, R. Rigny, R. Ben‐Aïm, Determination of the gas‐phase decomposition rate constants of heptyl‐1 and heptyl‐2 hydroperoxides $C_7H_{15}OOH$, Int. J. Chem. Kinet. 14 (1982) 1325-1337.
[38] A.D. Kirk, J.H. Knox, The pyrolysis of alkyl hydroperoxides in the gas phase, Trans. Faraday Soc 56 (1960) 1296-1303.
[39] D. Baulch, C. Cobos, R. Cox, C. Esser, P. Frank, T. Just, J. Kerr, M. Pilling, J. Troe, R. Walker, Evaluated kinetic data for combustion modelling, J. Phys. Chem. Ref. Data 21 (1992) 411-734.
[40] C.F. Goldsmith, M.P. Burke, Y. Georgievskii, S.J. Klippenstein, Effect of non-thermal product energy distributions on ketohydroperoxide decomposition kinetics, Proc. Combust. Inst. 35 (2015) 283-290.
[41] D.M. Popolan-Vaida, A.J. Eskola, B. Rotavera, J.F. Lockyear, Z. Wang, S.M. Sarathy, R.L. Caravan, J. Zádor, L. Sheps, A. Lucassen, K. Moshammer, P. Dagaut, D.L. Osborn, N. Hansen, S.R. Leone, C.A. Taatjes, Formation of Organic Acids and Carbonyl Compounds in n-Butane Oxidation via γ-Ketohydroperoxide Decomposition, Angew. Chem. Int. Ed. Engl. 61 (2022) e202209168.
[42] L. Xing, J.L. Bao, Z. Wang, F. Zhang, D.G. Truhlar, Degradation of Carbonyl Hydroperoxides in the Atmosphere and in Combustion, J. Am. Chem. Soc. 139 (2017) 15821-15835.
[43] L.-S. Tran, O. Herbinet, H.-H. Carstensen, F. Battin-Leclerc, Chemical kinetics of cyclic ethers in combustion, Prog. Energy Combust. Sci. 92 (2022) 101019.
[44] A.C. Doner, J. Zádor, B. Rotavera, Stereoisomer-dependent unimolecular kinetics of 2,4-dimethyloxetanyl peroxy radicals, Faraday Discuss. 238 (2022) 295-319.
[45] A.C. Doner, M.M. Davis, A.L. Koritzke, M.G. Christianson, J.M. Turney, H.F. Schaefer, L. Sheps, D.L. Osborn, C.A. Taatjes, B. Rotavera, Isomer‐dependent reaction mechanisms of cyclic ether intermediates:cis‐2,3‐dimethyloxirane andtrans‐2,3‐dimethyloxirane, Int. J. Chem. Kinet. 53 (2020) 127-145.
[46] M.G. Christianson, A.C. Doner, M.M. Davis, A.L. Koritzke, J.M. Turney, H.F. Schaefer, L. Sheps, D.L. Osborn, C.A. Taatjes, B. Rotavera, Reaction mechanisms of a cyclic ether intermediate: Ethyloxirane, Int. J. Chem. Kinet. 53 (2020) 43-59.
[47] Y. Fenard, M.A. Boumehdi, G. Vanhove, Experimental and kinetic modeling study of 2-

methyltetrahydrofuran oxidation under engine-relevant conditions, Combust. Flame 178 (2017) 168-181.
[48] Y. Fenard, H. Song, H. Minwegen, P. Parab, C.S. Mergulhão, G. Vanhove, K.A. Heufer, 2,5-Dimethyltetrahydrofuran combustion: Ignition delay times at high and low temperatures, speciation measurements and detailed kinetic modeling, Combust. Flame 203 (2019) 341-351.
[49] G. Vanhove, Y. Yu, M.A. Boumehdi, O. Frottier, O. Herbinet, P.A. Glaude, F. Battin-Leclerc, Experimental Study of Tetrahydrofuran Oxidation and Ignition in Low-Temperature Conditions, Energy Fuels 29 (2015) 6118-6125.
[50] N. Hansen, K. Moshammer, A.W. Jasper, Isomer-Selective Detection of Keto-Hydroperoxides in the Low-Temperature Oxidation of Tetrahydrofuran, J. Phys. Chem. A 123 (2019) 8274-8284.
[51] E.R. Ritter, J.W. Bozzelli, THERM: Thermodynamic property estimation for gas phase radicals and molecules, Int. J. Chem. Kinet. 23 (1991) 767-778.
[52] CHEMKIN-PRO 15092, Reaction Design, San Diego, 2009.
[53] Z. Wang, D.M. Popolan-Vaida, B. Chen, K. Moshammer, S.Y. Mohamed, H. Wang, S. Sioud, M.A. Raji, K. Kohse-Höinghaus, N. Hansen, P. Dagaut, S.R. Leone, S.M. Sarathy, Unraveling the structure and chemical mechanisms of highly oxygenated intermediates in oxidation of organic compounds, Proc. Natl. Acad. Sci. U. S. A. 114 (2017) 13102-13107.
[54] Z.D. Wang, O. Herbinet, N. Hansen, F. Battin-Leclerc, Exploring hydroperoxides in combustion: History, recent advances and perspectives, Prog. Energy Combust. Sci. 73 (2019) 132-181.
[55] Z.D. Wang, L.D. Zhang, K. Moshammer, D.M. Popolan-Vaida, V.S.B. Shankar, A. Lucassen, C. Hemken, C.A. Taatjes, S.R. Leone, K. Kohse-Höinghaus, N. Hansen, P. Dagaut, S.M. Sarathy, Additional chain-branching pathways in the low-temperature oxidation of branched alkanes, Combust. Flame 164 (2016) 386-396.
[56] Z. Wang, S.M. Sarathy, Third O_2 addition reactions promote the low-temperature auto-ignition of *n*-alkanes, Combust. Flame 165 (2016) 364-372.
[57] A. Jalan, I.M. Alecu, R. Meana-Paneda, J. Aguilera-Iparraguirre, K.R. Yang, S.S. Merchant, D.G. Truhlar, W.H. Green, New pathways for formation of acids and carbonyl products in low-temperature oxidation: the Korcek decomposition of gamma-ketohydroperoxides, J. Am. Chem. Soc. 135 (2013) 11100-11114.
[58] S.J. Dong, K.W. Zhang, E.M. Ninnemann, A. Najjar, G. Kukkadapu, J. Baker, F. Arafin, Z.D. Wang, W.J. Pitz, S.S. Vasu, S.M. Sarathy, P.K. Senecal, H.J. Curran, A comprehensive experimental and kinetic modeling study of 1-and 2-pentene, Combust. Flame 223 (2021) 166-180.